



**HAL**  
open science

## High-Pressure Melting Curve of Zintl Sodium Silicide $\text{Na}_4\text{Si}_4$ by In Situ Electrical Measurements

Alexandre Courac, Yann Le Godec, Carlos Renero-Lecuna, Hicham Moutaabbid, Ram Kumar, Cristina Coelho-Diogo, Christel Gervais, David Portehault

► **To cite this version:**

Alexandre Courac, Yann Le Godec, Carlos Renero-Lecuna, Hicham Moutaabbid, Ram Kumar, et al.. High-Pressure Melting Curve of Zintl Sodium Silicide  $\text{Na}_4\text{Si}_4$  by In Situ Electrical Measurements. *Inorganic Chemistry*, 2019, 58 (16), pp.10822-10828. 10.1021/acs.inorgchem.9b01108 . hal-02342905

**HAL Id: hal-02342905**

**<https://hal.sorbonne-universite.fr/hal-02342905>**

Submitted on 10 Nov 2020

**HAL** is a multi-disciplinary open access archive for the deposit and dissemination of scientific research documents, whether they are published or not. The documents may come from teaching and research institutions in France or abroad, or from public or private research centers.

L'archive ouverte pluridisciplinaire **HAL**, est destinée au dépôt et à la diffusion de documents scientifiques de niveau recherche, publiés ou non, émanant des établissements d'enseignement et de recherche français ou étrangers, des laboratoires publics ou privés.

# High Pressure Melting Curve of Zintl Sodium Silicide Na<sub>4</sub>Si<sub>4</sub> by *In Situ* Electrical Measurements

*Alexandre Courac,<sup>\*,a</sup> Yann Le Godec,<sup>a</sup> Carlos Renero-Lecuna,<sup>a</sup> Hicham Moutaabbid,<sup>a</sup> Ram Kumar,<sup>b</sup> Cristina Coelho-Diogo,<sup>c</sup> Christel Gervais,<sup>b</sup> and David Portehault<sup>b</sup>*

<sup>a</sup> Sorbonne Université, CNRS, Muséum National d'Histoire Naturelle, IRD, Institut de Minéralogie, de Physique des Matériaux et de Cosmochimie (IMPMC), 75005 Paris, France

<sup>b</sup> Sorbonne Université, CNRS, Collège de France, Laboratoire de Chimie de la Matière Condensée de Paris (CMCP), 4 place Jussieu, F-75005, Paris, France

<sup>c</sup> Sorbonne Université, CNRS, Institut des Matériaux de Paris Centre, 4 place Jussieu, F-75005, Paris, France

AUTHOR INFORMATION

**Corresponding Author**

\* Corresponding author: alexandre.courac@upmc.fr

ABSTRACT. The inorganic chemistry of the Na-Si system at high pressure is fascinating, with a large number of interesting compounds accessible in the industrial pressure scale, below 10 GPa. Especially,  $\text{Na}_4\text{Si}_4$  is stable in this whole pressure range, and thus plays an important role for understanding the thermodynamics and kinetics underlying materials synthesis at high pressures and high temperatures. In the present work, the melting curve of the Zintl compound  $\text{Na}_4\text{Si}_4$  made of  $\text{Na}^+$  and  $\text{Si}_4^{4-}$  tetrahedral cluster ions is studied at high pressures up to 5 GPa, by using *in situ* electrical measurements. During melting, the insulating  $\text{Na}_4\text{Si}_4$  solid transforms into an ionic conductive liquid that can be probed through the conductance of the whole high-pressure cell, i.e. the system constituted of the sample, the heater and the high-pressure assembly.  $\text{Na}_4\text{Si}_4$  melts congruently in the studied pressure range and its melting point increases with pressure with a positive slope  $dT_m/dp$  of 20(4) K/GPa.

**KEYWORDS** Sodium silicide, High pressure, Phase diagram, Melting curve

## INTRODUCTION

The Zintl solid sodium silicide  $\text{Na}_4\text{Si}_4$  bears Si species with negative oxidation state and built on  $[\text{Si}_4]^{4-}$  tetrahedral clusters, which are surrounded by  $\text{Na}^+$  cations on each face.<sup>1-2</sup> The presence of both covalent and ionic bonds in the structure imparts interesting chemical and physical attributes.<sup>3</sup>  $\text{Na}_4\text{Si}_4$  itself may be considered as a strategic energy material in hydrogen technologies to generate hydrogen as a fuel (portable hydrogen fuel cell cartridges) and for high energy density storage of hydrogen under low pressure.<sup>4</sup> Besides,  $\text{Na}_4\text{Si}_4$  is a promising precursor for the synthesis of extended Si frameworks and allotropes of technological relevance.<sup>5-13</sup>  $\text{Na}_x\text{Si}_{46}$  ( $x \leq 8$ ) and  $\text{Na}_x\text{Si}_{136}$  ( $x \leq 24$ ) (type-I and type-II clathrates, respectively) consisting of Si cages encapsulating Na have been reported from  $\text{Na}_4\text{Si}_4$  decomposition.<sup>14-17</sup> Empty  $\text{Si}_{46}$  and  $\text{Si}_{136}$  frameworks also provide tunable band gap for thermoelectrics and photovoltaics with  $\text{Si}_{136}$  exhibiting a quasi-direct bandgap of  $\sim 2$  eV.<sup>15, 18</sup> Recently  $\text{Na}_4\text{Si}_4$  has been used as precursor to design a new high-pressure synthetic route to the narrow-bandgap silicon allotrope Si-III.<sup>13, 19</sup> As a starting material,  $\text{Na}_4\text{Si}_4$  is a compound of choice, as compared to ductile metallic sodium, for high pressure synthesis, since it can be finely powdered, which is crucial for homogeneity of the product. In addition, it participates in the phase equilibria<sup>11</sup> and impacts crystallization kinetics<sup>20</sup> in the binary Na-Si system that holds great promise to discover new technologically relevant semiconducting Si allotropes and compounds in the high pressure range. This is exemplified by the high pressure clathrate  $\text{NaSi}_6$ <sup>20-21</sup> that leads by Na subtraction to the new orthorhombic allotrope  $\text{Si}_{24}$  with quasi-direct bandgap of  $\sim 1.35$  eV,<sup>6</sup> making this solid highly relevant for energy conversion.<sup>22</sup> Overall,  $\text{Na}_4\text{Si}_4$  appears as an important starting or intermediate compound that participates in the Na-Si phase equilibria during high-pressure syntheses. However, our understanding of the high pressure-temperature phase diagram and more broadly of thermodynamic data of  $\text{Na}_4\text{Si}_4$  is incomplete and relies sometimes on controversial reports.<sup>23-25</sup>

Na<sub>4</sub>Si<sub>4</sub> at ambient pressure has two low- and high- temperature polymorphs,  $\alpha$ - and  $\beta$ - respectively.<sup>23,26</sup> The temperature of the  $\alpha$ -to- $\beta$  transformation is  $\sim 885$  K at ambient pressure.<sup>24</sup> An isosymmetric transformation of the monoclinic  $\alpha$  form has been also reported above 10 GPa and 300 K, yielding  $\gamma$ -Na<sub>4</sub>Si<sub>4</sub>.<sup>27</sup> The equation-of-state for  $\alpha$ -Na<sub>4</sub>Si<sub>4</sub> below 10 GPa<sup>27,28</sup> suggests a bulk modulus  $B_0 = 24(1)$  GPa ( $B'_0 = 4$ ). According to the density of the different polymorphs,  $\beta$ - and  $\gamma$ -Na<sub>4</sub>Si<sub>4</sub> should exhibit lower and higher bulk modulus, respectively, but still close to that of the  $\alpha$  form.<sup>29-32</sup>

In order to effectively use Na<sub>4</sub>Si<sub>4</sub> as precursor for high-pressure syntheses, a detailed understanding of its high pressure-temperature phase diagram and physical behavior in the liquid state is an important requisite. With this objective, we have especially focused on the melting curve of Na<sub>4</sub>Si<sub>4</sub>. Because of their refractory behavior and high reactivity, assessing melting of compounds like Na<sub>4</sub>Si<sub>4</sub> under HPHT conditions is a significant methodological challenge. Indeed, *in situ* X-ray diffraction (XRD) peaks are widened under HP and Na-Si solids and liquids react with most available thermocouples, thus hindering a precise evaluation of the melting temperature by regular XRD techniques. To overcome this limitation, we propose a new methodology to probe phase transitions, based on electrical conductivity measurements.

## EXPERIMENTAL METHODS

### *Synthesis*

The silicon ( $\sim 325$  mesh, 99%) and NaH (95%) powder were obtained from Sigma-Aldrich. All the synthesis and manipulations were performed inside a glove-box and on a Schlenk line under Ar atmosphere. Na<sub>4</sub>Si<sub>4</sub> was synthesized using a procedure adapted from the one

reported by Ma *et al.*<sup>33</sup> In a typical synthesis Si and NaH powders were mixed in 1:2.1 mole ratio and ball milled for 2 min at 20 Hz (Retsch MM400 ball mill airtight vials of 50 mL, one steel ball of 62.3 g and a diameter of 23 mm). The obtained homogeneous mixture was transferred to an h-BN crucible, covered with a lid and subsequently transferred inside a quartz tube. The reaction was performed at 420 °C for 90 hours under Ar. The product was obtained as a brown-black pellet with white residue on top. The white residue corresponded to NaOH and was carefully removed from the top of the pellet. The latter was crushed to obtain Na<sub>4</sub>Si<sub>4</sub> powder.

### *Characterization*

X-ray diffraction (XRD) was performed on a Bruker D8 Advance diffractometer operating at the Cu K $\alpha$  wavelength, with a sample holder equipped with a plastic dome to maintain the sample under inert argon atmosphere. The crystallographic reference was obtained from the reference ICSD card 193513. The resulting grey powder (according to XRD,  $a = 12.17(2)$  Å,  $b = 6.55(1)$  Å,  $c = 11.15(2)$  Å,  $\beta = 119.0(3)^\circ$ , space group No 15, C12/c1, which corresponds to the  $\alpha$ -Na<sub>4</sub>Si<sub>4</sub> polymorph)<sup>26</sup> was transferred and stored under argon. <sup>29</sup>Si and <sup>23</sup>Na magic angle spinning nuclear magnetic resonance (MAS NMR) experiments were performed on a 700 MHz AVANCE III Bruker spectrometer operating at 139.05 MHz using a 3.2 mm Bruker probe spinning at 20 kHz and at 185.20 MHz using a 4 mm Bruker probe spinning at 14 kHz respectively. A single-pulse excitation was used with a recycle delay of 500 s and 512 scans for <sup>29</sup>Si and of 1 s and 24 scans for <sup>23</sup>Na. <sup>29</sup>Si and <sup>23</sup>Na chemical shifts were referenced to TMS and 0.1M NaCl (aq) respectively. The spectra were simulated with the DMFIT program.<sup>34</sup>

### *Electrical measurements at HPHT*

High pressure experiments have been performed using an hydraulic “Paris-Edinburgh” (PE) press applying force on tungsten carbide opposite anvils that compress a high-pressure cell (Fig. 1a). High temperatures were achieved by resistive heating (graphite ceramic or plastified graphite material, Grafoil). The pressure was calibrated with the diamond Si equation-of-state by *in situ* XRD at the PSICHE beamline of synchrotron SOLEIL.<sup>11</sup> The temperature was calibrated with a Si melting standard at high pressure.<sup>35</sup> Graphite (as ceramic or in grafoil) is a material of choice to serve simultaneously as heater and capsule material, while being chemically inert versus the Na<sub>4</sub>Si<sub>4</sub> melt at the temperatures of interest. A typical HP cell is shown in Fig. 1a, along with the corresponding equivalent circuit (Fig. 1c) used for electrical measurements, including the heater and the sample (in parallel connection to the middle part of the heater). An alternating current was used for heating the cell by the Joule effect, simultaneously, the total resistance of the heating chain (together with voltage, current and power) has been probed. Figure 1b shows the theoretically expected power-resistance curves in the case of metallic and graphite heaters for insulator-to-metal transformations.

The HPHT experiments of simultaneous *in situ* XRD and electrical measurements has been performed at ID06 beamline at ESRF using large-volume multianvil press.<sup>36</sup> Ceramic graphite has been used as a heating material, with non linear heating (Fig. 1d). Figures 1d and 1e show the validity of the methodology, i.e. the correlation of the resistance drop with changes in powder diffraction patterns using *R-t*, *P-t* and XRD vs time diagrams. However, constant (preferably linear power change) heating rate has to be used for reliable analysis to exclude artefacts non-related to sample electrical properties (e.g. green arrow on Fig. 1d and e). Ceramic graphite is also then the best materials. In the following experiments, we have favored the use of grafoil, which allows obtaining smooth *R-P* curves.

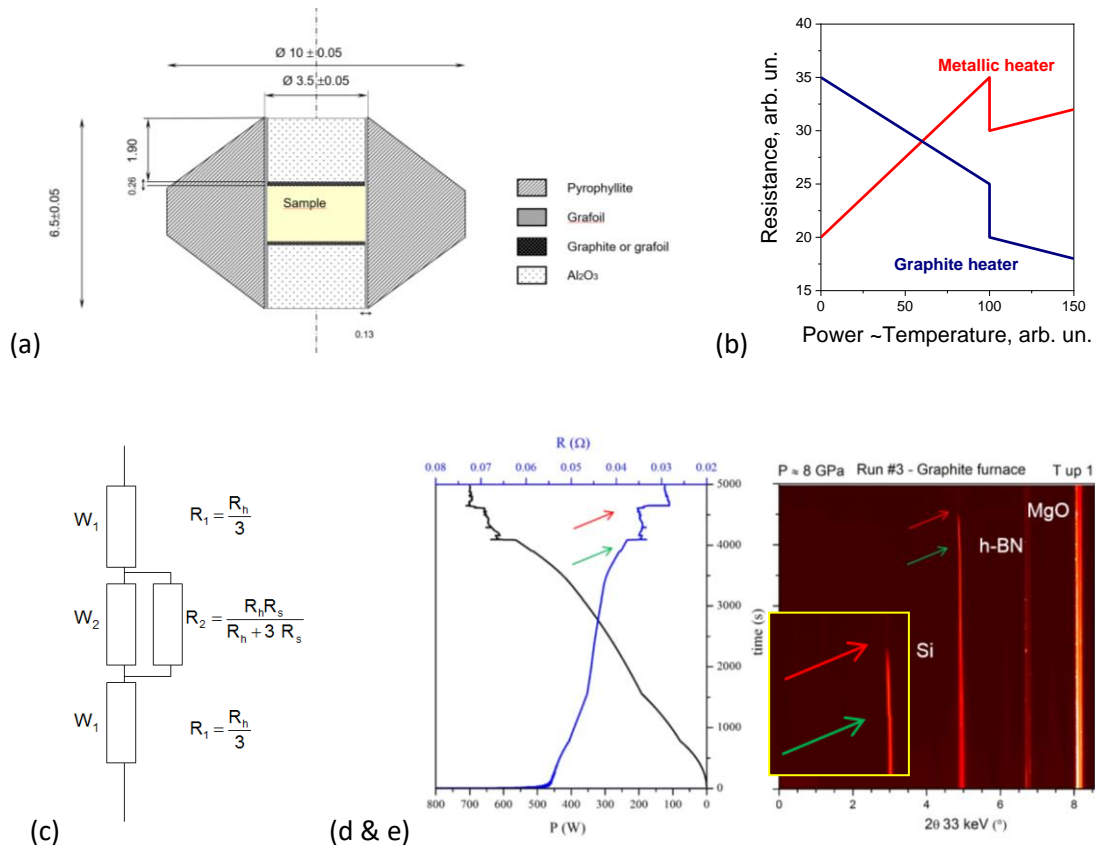
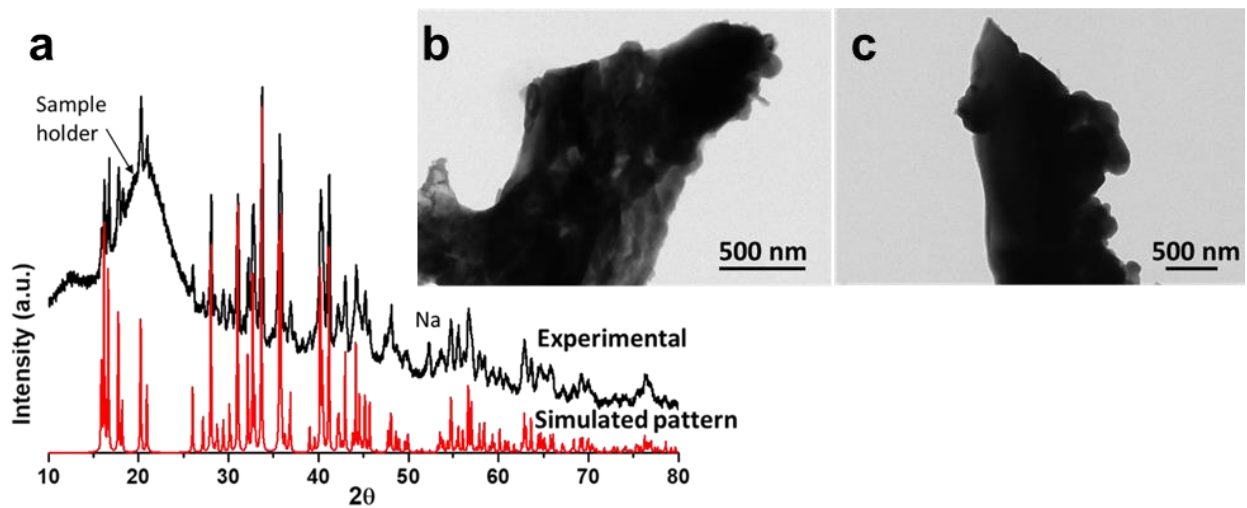


**Figure 1.** (a) High-pressure PE cell 10/3.5 for the electrical measurements of the (sample + heater) system. (b) Theoretical resistance curves of (sample + heater). The sample is an insulator below the critical power of 100 arb. un. and conducting, metallic above. (c) Electrical equivalent circuit of the (sample + heater) system with total resistance  $2R_1 + R_2$  ( $R_h$  – total heater resistance,  $R_s$  – sample resistance). (d & e) Simultaneous electrical ( $R$  and  $P$  vs  $t$ ) and in situ XRD measurements of Si in the ceramic graphite heater, as an example of the methodology. The vertical axes in **d** and **e** represent time with (non-linear) heating above silicon melting temperature (**d**). Arrows indicate the simultaneous changes in resistance and XRD patterns. Inset in **e** is a zoom-in showing changes in the  $d$ -spacing of Si reflection: the red arrows correspond to melting. The green arrows are most probably due to a slight pressure drop.

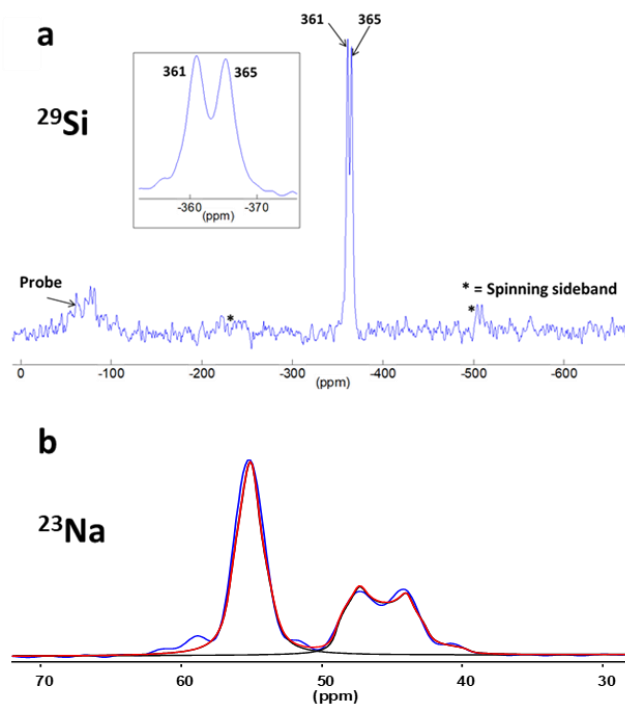
## RESULTS



The Na<sub>4</sub>Si<sub>4</sub> compound studied in the present work was synthesized by reaction between sodium hydride and silicon. The XRD pattern (Fig. 2a) measured under inert atmosphere shows that Na<sub>4</sub>Si<sub>4</sub> is the main phase, with trace amounts of Na and NaOH. TEM (Fig. 2b,c) shows that the particles are micron-size. The <sup>29</sup>Si MAS solid state NMR spectrum of Na<sub>4</sub>Si<sub>4</sub> (Fig. 3a) shows signals at 361 and 365 ppm in excellent agreement with previously reported data<sup>37</sup> and corresponding to the two crystallographically different Si sites in the crystal structure (monoclinic, *C2/c*).<sup>3</sup> The upfield shift compared to pure silicon or silicon oxides is attributed to the electron donation from the electropositive Na to the electronegative Si.<sup>38</sup> Similarly, the <sup>23</sup>Na spectrum (Fig. 3b) shows two quadrupolar resonance patterns in nearly equal proportions and with isotropic chemical shift values of 56.5 ppm (*Cq* = 1.27 MHz, *η* = 0.8) and 49.7 ppm (*Cq* = 2.34 MHz, *η* = 0.25), corresponding to two crystallographically different Na sites in the crystal structure. The quadrupolar parameters of the two sites are significantly different, suggesting differences for the two sites in terms of electronic and symmetry environments. An additional signal on the <sup>23</sup>Na NMR spectrum, at ca. 20 ppm, corresponds to impurities and accounts for approximately 5% of the total amount of Na. It can be possibly assigned to NaOH.<sup>39</sup>



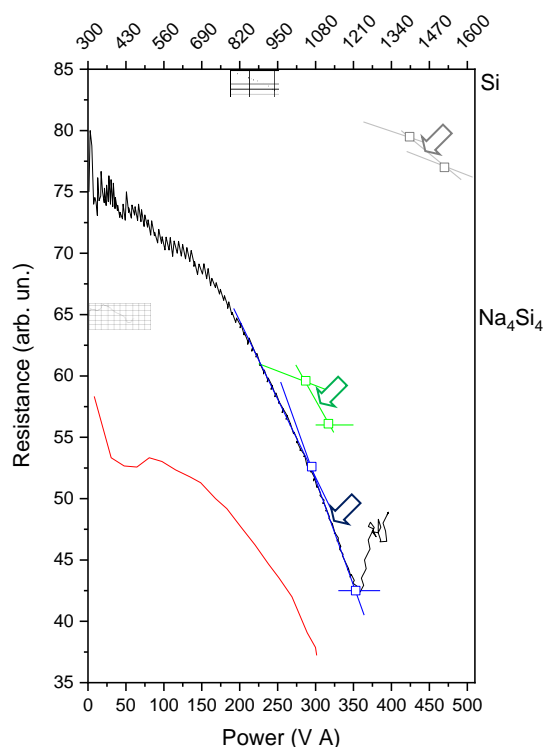
**Figure 2.** (a) Powder XRD pattern (black) of as-obtained  $\text{Na}_4\text{Si}_4$ . The calculated reference pattern for  $\text{Na}_4\text{Si}_4$  is shown in red. A peak at  $\sim 52^\circ$  corresponds to metallic sodium impurities. (b, c) TEM images of as-synthesized  $\text{Na}_4\text{Si}_4$ .



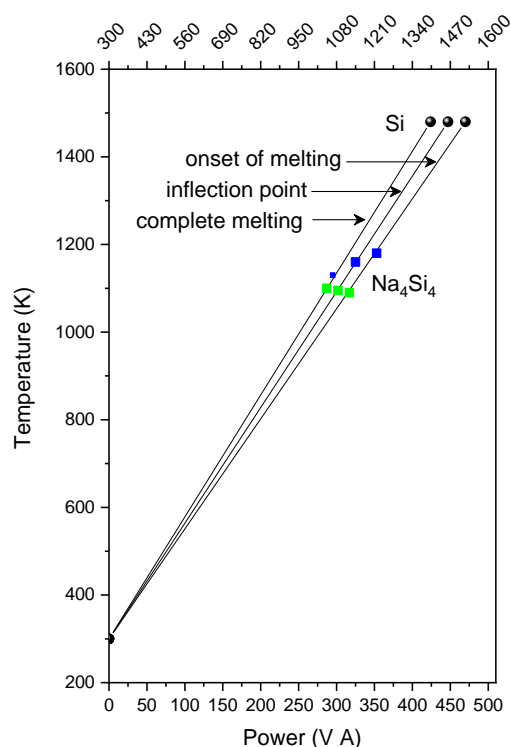
**Figure 3.** (a)  $^{29}\text{Si}$  and (b)  $^{23}\text{Na}$  solid-state NMR spectra of as-obtained  $\text{Na}_4\text{Si}_4$ .

Figure 4a shows typical power-resistance ( $P$ - $R$ ) curves for Si and  $\text{Na}_4\text{Si}_4$ . In the case of Si the  $P$ - $R$  dependence prior to melting follows a quasi-linear decrease, typical for plastified grafoil.

Here we should note that in the case of ceramic graphite, the dependence is never so smooth, most probably because of the cracking of ceramics under pressure and, thus, of the modification of electrical contacts. Metallic heaters-capsules behave similar to grafoil, but with a quasi-linear increase of resistance. The Si *P-R* curve allows distinguishing three points related to melting: (1) onset, (2) inflection and (3) accomplishing melting powers. Each specific power cannot be attributed to a single temperature due to the temperature gradients inside the HP cell. Each of the three characteristic points on melting curve can be used for temperature calibration, thus resulting in three calibration curves (Fig. 4b). We favor the use of the inflection point as the best estimate, while onset and accomplishing points allow estimating the error bar. Actually, the three calibration curves just represent three different places in the cell: the hottest, intermediate and coldest places.



(a)



(b)

**Figure 4. (a)** Experimental resistance curves of the ( $\text{Na}_4\text{Si}_4$  + heater) system at 2, 4 and 5 GPa (green, red and blue eye-guide lines, respectively). The Si sample has been used as a temperature standard (melting at 1480 K at 4 GPa). The non-linear resistance behavior in ( $\text{Na}_4\text{Si}_4$  + grafoil) system as compared to (Si + grafoil) can be explained by smaller hardness of  $\text{Na}_4\text{Si}_4$  (and, therefore, higher deformation of the heater) and increase of the solid-state ionic conductivity when approaching melting. Arrows of corresponding color show the points attributed to the melting. The squiggles appear at the end of some curves because the power-resistance points are connected at increasing time, while the resistance may change at constant power during heating. **(b)** Silicon calibration curve (from the position of inflection point,  $T = 300 + 2.64 \times P$ ) and temperature estimation of the  $\text{Na}_4\text{Si}_4$  melting point at different pressures from onset, inflection and completion points on the resistance curves (2 and 5 GPa by green and blue squares, respectively).

The electrical behavior of  $\text{Na}_4\text{Si}_4$  under heating is different from the ideal case of Si (Fig. 4a). The typical feature of melting can be clearly distinguished (green and blue lines allow distinguishing clearly the onset, inflection and completion points) by a change in the slope of resistance =  $f(\text{power})$  curves. Similar to silicon,  $\text{Na}_4\text{Si}_4$  is an insulator in the solid state (covalent Si and ionic  $\text{Na}_4\text{Si}_4$  solids) and conductor in the liquid state (metallic Si and  $\text{Na}_4\text{Si}_4$  ionic liquids). Visual analysis of recovered samples indicates that a transient drop of the resistance with subsequent increase in the resistance-power curve is characteristic of melting (black  $\text{Na}_4\text{Si}_4$  curves at Fig. 4a, black circles at Fig. 5a). On the contrary, a strong resistance drop without subsequent resistance increase (red  $\text{Na}_4\text{Si}_4$  curve at Fig. 4a, grey circle at Fig. 5a) cannot definitively indicate the melting (no melting features in recovered sample). The mechanism of such behavior is not clear so far, but no interaction between sodium silicide and graphite was observed at the temperatures studied. No correlation with a possible  $\alpha$ -to- $\beta$

transformation could be evidenced either. All in all, the melting curve of  $\text{Na}_4\text{Si}_4$  could be extracted (Fig. 5a) from the 2 and 5 GPa resistance curves (Fig. 4a). Theoretically, ionic conductivity can be evaluated from such experiments.<sup>40</sup> For such estimation the knowledge of sample size and shape during melting is crucial. However, in our case the powder was used as starting material, making it impossible to evaluate the sample dimensions under compression. Combined synchrotron X-ray imaging and electrical measurements on a sintered  $\text{Na}_4\text{Si}_4$  sample could resolve this problem, but outstands the scope of the present work. One also needs to comment on the possible impact of contaminations (e.g. Na, NaOH mentioned above) on the melting temperature. The melt, once formed, enters into contact with the heater and/or escapes the central part of the HP cell with highest pressure. However, the quantity of Na and NaOH impurities and of related possible eutectic liquids corresponding to a maximum of about 5 mol. % of the total amount of Na, as evaluated from NMR. These amounts are so small that only the melting of the sample whole volume can cause noticeable resistance change (typically ~20-30% change observed herein). Possible chemical reactions with graphite may have occurred, but to a minor extent, as the heaters were always recovered after the experiments as being deformed, with no visible reaction on their walls. Such contaminations melting(s) and side reactions with the heater container may be responsible for the significant noise observed on the resistance curve at the initial heating stage (e.g. below 150 VA, Fig. 4a), which occurs in the domain of melting temperatures of these impurities. However, they cannot be account for the significant resistance drop observed at higher temperature, which we attribute to  $\text{Na}_4\text{Si}_4$  melting.

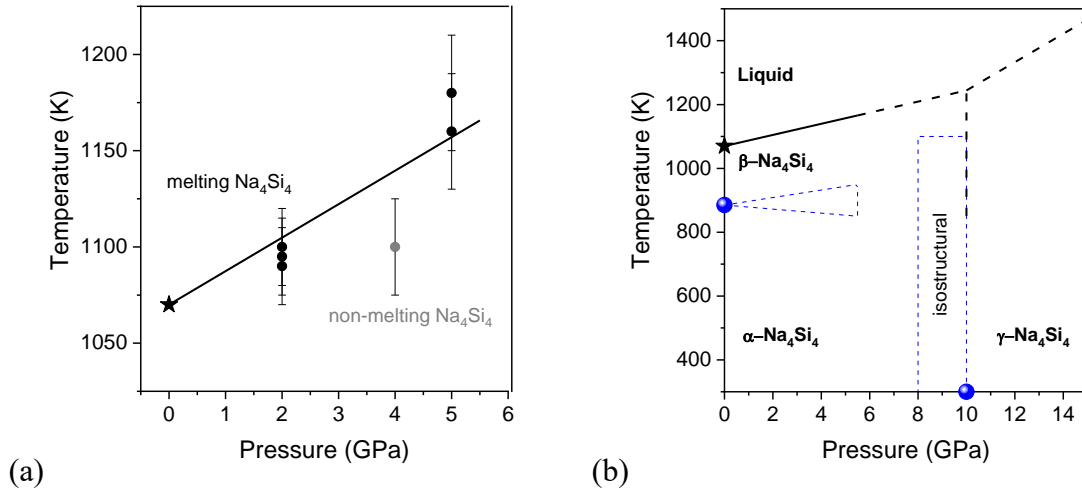


**Figure 5. (a)** Experimental melting curve of Na<sub>4</sub>Si<sub>4</sub>. The  $T_m - p$  dependence is quasilinear (solid line) and follows the equation  $T_m(\text{K}) = 1070 + 17.4 \times p(\text{GPa})$  (the best estimate for linear dependence of melting curve has been obtained by weighted least square fit.). **(b)** High-pressure, high-temperature data on the phase diagram of Na<sub>4</sub>Si<sub>4</sub>. Solid symbols show the experimental data available from 24, 27. The solid line indicates the results of the present work. Blue dashed lines (guides for eye) delimit possible domains of localization of  $\alpha/\beta$  and  $\alpha/\gamma$  (observed experimentally)<sup>27</sup> equilibrium lines. Black dashed lines show extrapolated equilibria  $\alpha/\text{liquid}$  and  $\alpha/\gamma$  together with tentative  $\gamma/\text{liquid}$  line.

## DISCUSSION

The positive slope of the melting curve of Na<sub>4</sub>Si<sub>4</sub> is  $dT_m/dp = +17(2) \text{ K GPa}^{-1}$ , which is indicative of positive melting volume change of  $\Delta V_m = \Delta H_m \times (dT_m/dp) / T_m$ . Using the estimation of  $\Delta H_m \sim 204 \text{ kJ/mol}$ ,<sup>23, 41</sup> one can evaluate  $\Delta V_m \sim 3.3 \text{ cm}^3 \text{ mol}^{-1}$  (or atomic volume change of  $0.41 \text{ cm}^3 \text{ mol}^{-1}$ ). It is interesting to note that Si itself shows negative  $dT_m/dp = -60 \text{ K GPa}^{-1}$ ,<sup>35</sup> and  $\Delta V_m = -1.8 \text{ cm}^3 \text{ mol}^{-1}$  according to thermochemical data ( $\Delta H_m = 50.2 \text{ kJ mol}^{-1}$ )<sup>41</sup>, while direct experimental measurements give  $\Delta V_m = -(1.4-1.9) \text{ cm}^3/\text{mol}$ .<sup>42-43</sup> Such a

negative dependence is typical for diamond-type crystal structures.<sup>44-45</sup> Sodium shows  $dT_m/dp = 87 \text{ K/GPa}$ ,<sup>46</sup> which combines with  $\Delta H_m = 2.6 \text{ kJ mol}^{-1}$  to give  $\Delta V_m = +0.61 \text{ cm}^3 \text{ mol}^{-1}$ , close to experimentally observed  $+0.6 \text{ cm}^3 \text{ mol}^{-1}$ .<sup>47</sup>

Fig. 6 shows a non-linear dependence of the melting volume on the composition. Such a non-trivial dependence is related to the diversity of chemical species present in the solids and liquid.  $\text{Na}_4\text{Si}_4$  liquid encompasses  $[\text{Si}_4]^{4-}$  polyhedral clusters that do not allow significant volume decrease, in contrast with pure Si with significant difference in packings between solid diamond and atomic liquid structures. Also, if one follows the guide-for-the-eye curve (Fig. 6), the melting volume change for clathrate compounds in the Na-Si system are expected to be close to zero, which is to be confirmed (or refuted) experimentally. Theoretical simulations of open-framework Si clathrates suggest their strongly negative melting slopes<sup>48-49</sup> due to a dense liquid phase similar to ambient pressure Si liquid, thus rendering the clathrates (open frameworks + intercalated atoms) also strongly negative  $\Delta V_m$  – even probably more than Si – if Si in Na-Si liquids has local structure similar to Si rather than clathrate-related structure(s).

**Table 1.** Thermodynamic data on melting of Na,  $\text{Na}_4\text{Si}_4$  and Si. Bold values represent the experimental data from this work, non-bold values show the data from previous works (values given in italic – obtained by *ab initio* calculations).

Phase	$dT_m/dp$ , K/GPa	$\Delta H_m$ , kJ mol <sup>-1</sup>	$\Delta V_m^{\text{calculated}}$ , cm <sup>3</sup> mol <sup>-1</sup>	$\Delta V_m^{\text{experimental}}$ , cm <sup>3</sup> mol <sup>-1</sup>	$T_m$ , K at 0.1 MPa
Na	87(7)	2.6	+0.61(5)	+0.6	371
$\text{Na}_4\text{Si}_4$	<b>+17(2)</b>	8×25.5	+8× <b>0.41</b>	--	1070
Si	-60(7)	50.2	-1.8(2)	-1.4 to -1.9	1687

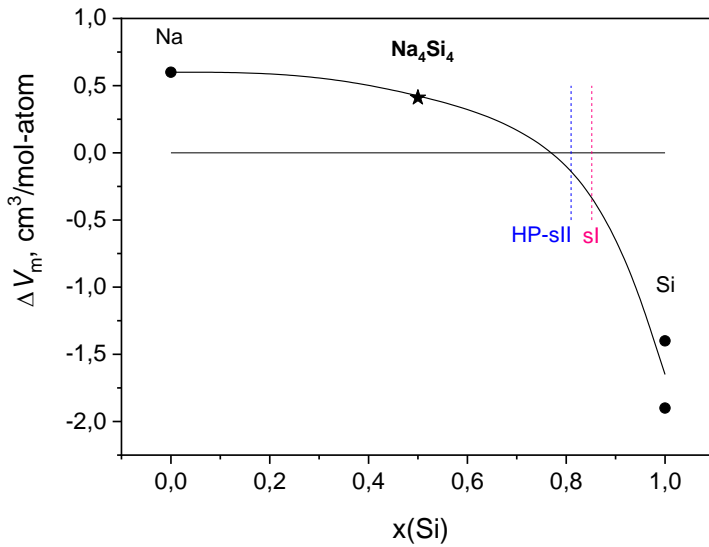


**Figure 6.** Melting volume  $\Delta V_m$  (per mole of atoms, at melting temperature) of  $\text{Na}_4\text{Si}_4$ , in comparison with experimental values for  $\text{Na}$ <sup>47</sup> and  $\text{Si}$ .<sup>42-43</sup> The continuous thick black curve is a guide for the eye. The thin solid horizontal line corresponds to  $\Delta V = 0$ ; while the blue and red dashed vertical lines show the composition of  $\text{Na}_{30.5}\text{Si}_{136}$  (HP-sII) and  $\text{Na}_8\text{Si}_{46}$  (sI) clathrates respectively.

The established melting curve is shown as a black solid line on the tentative phase diagram of  $\text{Na}_4\text{Si}_4$  at HPHT conditions (Fig. 5b). Linear extrapolation of the melting curve to high pressures and its intersection with the 10 GPa isobar (corresponding to the room-temperature isosymmetric (isostructural)  $\alpha$ -to- $\gamma$  transformation, which should be of first order (or discontinuous) with  $\Delta V \neq 0$ )<sup>50</sup>, allows giving the first estimate for a triple point of  $\text{Na}_4\text{Si}_4$  at  $\sim 10$  GPa and  $\sim 1250$  K. For high-pressure synthesis, the importance of this triple point for syntheses at  $\sim 10$  GPa may be very high. Additional *in situ* studies are then required to probe the phase diagram of  $\text{Na}_4\text{Si}_4$  at such high pressures. In order to get thermodynamically



consistent estimate for the melting curve of Na<sub>4</sub>Si<sub>4</sub> above 10 GPa (melting of  $\gamma$ -phase), we have used the high-temperature approximation (previously used, for example, for the construction of high-temperature part of boron phase diagram<sup>51</sup>), suggesting constant  $\Delta V$ ,  $\Delta H$  and  $\Delta S$  for such couple of phases. The only lacking value  $\Delta V_{\alpha/\gamma} = -8 \times 0.32 \text{ cm}^3 \text{ mol}^{-1}$ , that cannot be established as a combination of known values (using relationships  $\Delta X_{x/y} = -\Delta X_{y/z}$  and  $\Delta X_{x/y} = \Delta X_{x/z} + \Delta X_{z/y}$ ), has been established using experimental data.<sup>27</sup>

The above reported results also shed some light on the mechanism of synthesis of Na-Si clathrates at HPHT conditions, observed in previous *in situ* and *ex situ* experiments.<sup>11</sup> In fact, the formation of a high-pressure clathrate compound Na<sub>30.5</sub>Si<sub>136</sub> of structural type II encapsulating two sodium atoms in the same silicon polyhedral cages<sup>52</sup> (as compared to one atom in the case of stoichiometric Na<sub>24</sub>Si<sub>136</sub> compound) has been observed at temperatures  $\sim 300$  K below the melting point of Na<sub>4</sub>Si<sub>4</sub> (i.e. at  $\sim 800$  K).<sup>11</sup> The experimentally established eutectic melting temperature (equilibrium Na<sub>4</sub>Si<sub>4</sub>+Si $\leftrightarrow$ liquid) is just  $\sim 50$  K lower than that for pure Na<sub>4</sub>Si<sub>4</sub>,<sup>24</sup> which is indicative of the solid state interaction between Si and Na<sub>4</sub>Si<sub>4</sub> at temperatures below melt formation.

As a Zintl compound, Na<sub>4</sub>Si<sub>4</sub> is built from Na<sup>+</sup> cations and [Si<sub>4</sub>]<sup>4-</sup> clusters isostructural to the P<sub>4</sub> molecule constituting white phosphorus ( $\alpha$  wP). Hence, Na<sub>4</sub>Si<sub>4</sub> is an ionic solid, while  $\alpha$  wP is a molecular solid. Interestingly, the differences in properties of Na<sub>4</sub>Si<sub>4</sub> derived from our study and those reported for  $\alpha$  wP are consistent with the differences in cohesion. As expected, the ionic cohesion of Na<sub>4</sub>Si<sub>4</sub> provides it with much lower point melting point at 1080 K than the molecular solid  $\alpha$  wP at 317 K.<sup>53-54</sup> Likewise, our work indicates that the ionic solid Na<sub>4</sub>Si<sub>4</sub> has a melting slope of 20 K/GPa, ten times lower than the molecular solid  $\alpha$  wP.<sup>53-54</sup> Previous high pressure studies have also shown that the bulk modulus of  $\alpha$  wP is  $\sim 6.7(5)$  GPa,<sup>53</sup> while the presence of Na<sup>+</sup> ions distributed between the negatively charged

silicon tetrahedral leads to more than three times lower compressibility with bulk modulus of 24 GPa.

## CONCLUSIONS

Finally, the melting curve of  $\text{Na}_4\text{Si}_4$  has been established using the methodology of total resistance measurements (graphite or grafoil heater and sample in parallel electrical connection scheme). This method allows overpassing the problems of high reactivity (with electrodes or environment) and low crystal symmetry with polymorphism (for reliable XRD observation). Our results have shown the positive slope of  $\text{Na}_4\text{Si}_4$  melting curve, while the estimated value of the melting volume is close to that of sodium. Our results allow predicting a triple point of the liquid/ $\alpha$ / $\gamma$  phases at  $\sim 10$  GPa and 1250 K, i.e. potentially in the domain of interest for the synthesis of high-pressure intermetallic clathrates and silicon allotropes.

## ACKNOWLEDGMENT

We thank Mss. Silvia Pandolfi for assistance in high-pressure experiments. The work of A.C. was financially supported by Institut Universitaire de France (IUF). C.R.L. and D.P. thanks LabEx MATISSE program AAP 2016 - POST-DOCTORANTS. D.P. and R.K. thank the CNRS for funding. The French Région Ile de France - SESAME program is acknowledged for financial support (700 MHz NMR spectrometer). The *in situ* XRD experiments were performed on beamline ID06-LVP at the European Synchrotron Radiation Facility (proposal CH-5431). We are grateful to Drs. W. Crichton and K. Spector at the ESRF for providing assistance in using beamline ID06-LVP.

## REFERENCES

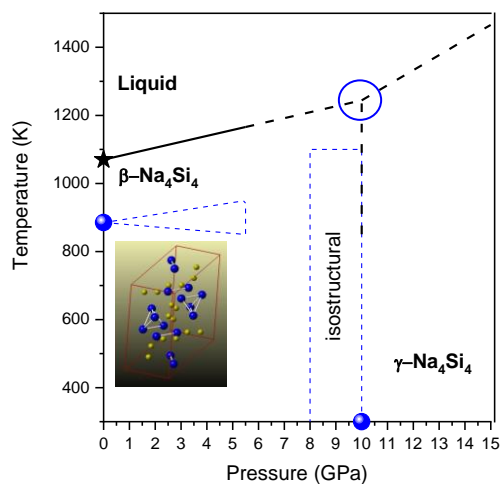
1. Nesper, R., Bonding Patterns in Intermetallic Compounds. *Angewandte Chemie International Edition in English* **1991**, *30* (7), 789-817.
2. Fässler, T. F., *Zintl Ions: Principles and Recent Developments* Springer Berlin Heidelberg, 2011.
3. Goebel, T.; Prots, Y.; Haarmann, F., Refinement of the crystal structure of tetrasodium tetrasilicide, Na<sub>4</sub>Si<sub>4</sub>. *Zeitschrift für Kristallographie - New Crystal Structures* **2008**, *223* (3), 187.
4. Agrawal, T.; Ajitkumar, R.; Prakash, R.; Nandan, G., Sodium Silicide As A Hydrogen Source For Portable Energy Devices: A Review. *Materials Today: Proceedings* **2018**, *5* (2, Part 1), 3563-3570.
5. Iversen, B. B.; Palmqvist, A. E. C.; Cox, D. E.; Nolas, G. S.; Stucky, G. D.; Blake, N. P.; Metiu, H., Why are Clathrates Good Candidates for Thermoelectric Materials? *Journal of Solid State Chemistry* **2000**, *149* (2), 455-458.
6. Kim, D. Y.; Stefanoski, S.; Kurakevych, O. O.; Strobel, T. A., Synthesis of an open-framework allotrope of silicon. *Nat. Mater.* **2015**, *14* (2), 169-173.
7. Kume, T.; Ohashi, F.; Nonomura, S., Group IV clathrates for photovoltaic applications. *Japanese Journal of Applied Physics* **2017**, *56* (5S1), 05DA05.
8. Connetable, D.; Timoshevskii, V.; Masenelli, B.; Beille, J.; Marcus, J.; Barbara, B.; Saitta, A. M.; Rignanese, G. M.; Melinon, P.; Yamanaka, S.; Blase, X., Superconductivity in Doped sp<sup>3</sup> Semiconductors: The Case of the Clathrates. *Phys. Rev. Lett.* **2003**, *91* (24), 247001.
9. Wang, Q.; Xu, B.; Sun, J.; Liu, H.; Zhao, Z.; Yu, D.; Fan, C.; He, J., Direct Band Gap Silicon Allotropes. *J. Amer. Chem. Soc.* **2014**, *136* (28), 9826-9829.
10. Kurakevych, O. O.; Le Godec, Y.; Crichton, W. A.; Strobel, T. A., Silicon allotropy and chemistry at extreme conditions. *Energy Procedia* **2016**, *92*, 839-844.
11. Jouini, Z.; Kurakevych, O. O.; Moutaabbid, H.; Le Godec, Y.; Mezouar, M.; Guignot, N., Phase boundary between Na-Si clathrates of structures I and II at high pressures and high temperatures. *J. Superhard Mater.* **2016**, *38* (1), 66-70.
12. Kurakevych, O. O.; Le Godec, Y.; Crichton, W. A.; Guignard, J.; Strobel, T. A.; Zhang, H. D.; Liu, H. Y.; Diogo, C. C.; Polian, A.; Menguy, N.; Juhl, S. J.; Alem, N.; Gervais, C., Synthesis of Bulk BC8 Silicon Allotrope by Direct Transformation and Reduced-Pressure Chemical Pathways (v6ol 55, pg 8943, 2016). *Inorg. Chem.* **2016**, *55* (19), 9949-9949.
13. Kurakevych, O. O.; Le Godec, Y.; Crichton, W. A.; Guignard, J.; Strobel, T. A.; Zhang, H. D.; Liu, H. Y.; Diogo, C. C.; Polian, A.; Menguy, N.; Juhl, S. J.; Gervais, C., Synthesis of Bulk BC8 Silicon Allotrope by Direct Transformation and Reduced-Pressure Chemical Pathways. *Inorg. Chem.* **2016**, *55* (17), 8943-8950.
14. Kasper, J. S.; Hagenmul, P.; Pouchard, M.; Cros, C., Clathrate Structure of Silicon and Na<sub>x</sub>Si<sub>136</sub> (x=11). *Science* **1965**, *150* (3704), 1713-1714.
15. Himeno, R.; Kume, T.; Ohashi, F.; Ban, T.; Nonomura, S., Optical absorption properties of Na<sub>x</sub>Si<sub>136</sub> clathrate studied by diffuse reflection spectroscopy. *Journal of Alloys and Compounds* **2013**, *574*, 398-401.
16. Simon, P.; Tang, Z.; Carrillo-Cabrera, W.; Chiong, K.; Böhme, B.; Baitinger, M.; Lichte, H.; Grin, Y.; Guloy, A. M., Synthesis and Electron Holography Studies of Single Crystalline Nanostructures of Clathrate-II Phases K<sub>x</sub>Ge<sub>136</sub> and Na<sub>x</sub>Si<sub>136</sub>. *Journal of the American Chemical Society* **2011**, *133* (19), 7596-7601.
17. Ramachandran, G. K.; Dong, J.; Diefenbacher, J.; Gryko, J.; Marzke, R. F.; Sankey, O. F.; McMillan, P. F., Synthesis and X-Ray Characterization of Silicon Clathrates. *Journal of Solid State Chemistry* **1999**, *145* (2), 716-730.

18. Gryko, J.; McMillan, P. F.; Marzke, R. F.; Ramachandran, G. K.; Patton, D.; Deb, S. K.; Sankey, O. F., Low-density framework form of crystalline silicon with a wide optical band gap. *Physical Review B* **2000**, *62* (12), R7707-R7710.
19. Zhang, H. D.; Liu, H. Y.; Wei, K. Y.; Kurakevych, O. O.; Le Godec, Y.; Liu, Z. X.; Martin, J.; Guerrette, M.; Nolas, G. S.; Strobel, T. A., BC8 Silicon (Si-III) is a Narrow-Gap Semiconductor. *Phys. Rev. Lett.* **2017**, *118* (14), 6.
20. Guerrette, M.; Ward, M. D.; Lokshin, K. A.; Wong, A. T.; Zhang, H. D.; Stefanoski, S.; Kurakevych, O.; Le Godec, Y.; Juhl, S. J.; Alem, N.; Fei, Y. W.; Strobel, T. A., Synthesis and Properties of Single-Crystalline Na<sub>4</sub>Si<sub>24</sub>. *Cryst. Growth Des.* **2018**, *18* (12), 7410-7418.
21. Kurakevych, O. O.; Strobel, T. A.; Kim, D. Y.; Muramatsu, T.; Struzhkin, V. V., Na-Si Clathrates Are High-Pressure Phases: A Melt-Based Route to Control Stoichiometry and Properties. *Cryst. Growth Des.* **2013**, *13* (1), 303-307.
22. Linghu, J.; Shen, L.; Yang, M.; Xu, S.; Feng, Y. P., Si<sub>24</sub>: An Efficient Solar Cell Material. *The Journal of Physical Chemistry C* **2017**, *121* (29), 15574-15579.
23. Hao, D.; Bu, M.; Wang, Y.; Tang, Y.; Gao, Q.; Wang, M.; Hu, B.; Du, Y., THERMODYNAMIC MODELING OF THE Na-X (X = Si, Ag, Cu, Cr) SYSTEMS. *J. Min. Metall. Sect. B* **2012**, *48* (2), 273 - 282.
24. Morito, H.; Yamada, T.; Ikeda, T.; Yamane, H., Na-Si binary phase diagram and solution growth of silicon crystals. *Journal of Alloys and Compounds* **2009**, *480* (2), 723-726.
25. Mali, A.; Petric, A., EMF Measurements of the Na-Si System. *Journal of Phase Equilibria and Diffusion* **2013**, *34* (6), 453-458.
26. Hohmann, E., Silicides and Germanides of the Alkali Metals. *Z. Anorg. Chem.* **1948**, *257* (1-3), 113-126.
27. Cabrera, R. Q.; Salamat, A.; Barkalov, O. I.; Leynaud, O.; Hutchins, P.; Daisenberger, D.; Machon, D.; Sella, A.; Lewis, D. W.; McMillan, P. F., Pressure-induced structural transformations of the Zintl phase sodium silicide. *Journal of Solid State Chemistry* **2009**, *182* (9), 2535-2542.
28. Murnaghan, F. D., The compressibility of media under extreme pressures. *Proct. Natl. Acad. Sci.* **1944**, *30*, 244.
29. Le Godec, Y.; Kurakevych, O. O.; Munsch, P.; Garbarino, G.; Solozhenko, V. L., Equation of state of orthorhombic boron, gamma-B-28. *Solid State Commun.* **2009**, *149* (33-34), 1356-1358.
30. Mukhanov, V. A.; Kurakevych, O. O.; Solozhenko, V. L., The interrelation between hardness and compressibility of substances and their structure and thermodynamic properties. *J. Superhard Mater.* **2008**, *30* (6), 368-378.
31. Solozhenko, V. L.; Kurakevych, O. O.; Le Godec, Y.; Brazhkin, V. V., Thermodynamically Consistent p-T Phase Diagram of Boron Oxide B<sub>2</sub>O<sub>3</sub> by in Situ Probing and Thermodynamic Analysis. *J. Phys. Chem. C* **2015**, *119* (35), 20600-20605.
32. Kurakevych, O. O.; Solozhenko, V. L., 300-K equation of state of rhombohedral boron subnitride, B<sub>13</sub>N<sub>2</sub>. *Solid State Commun.* **2009**, *149* (47-48), 2169-2171.
33. Ma, X.; Xu, F.; Atkins, T. M.; Goforth, A. M.; Neiner, D.; Navrotsky, A.; Kauzlarich, S. M., A versatile low temperature synthetic route to Zintl phase precursors: Na<sub>4</sub>Si<sub>4</sub>, Na<sub>4</sub>Ge<sub>4</sub> and K<sub>4</sub>Ge<sub>4</sub> as examples. *Dalton Trans.* **2009**, (46), 10250-10255.
34. Massiot, D.; Fayon, F.; Capron, M.; King, I.; Le Calvé, S.; Alonso, B.; Durand, J.-O.; Bujoli, B.; Gan, Z.; Hoatson, G., Modelling one- and two-dimensional solid-state NMR spectra. *Magnetic Resonance in Chemistry* **2002**, *40* (1), 70-76.
35. Kubo, A.; Wang, Y.; Runge, C. E.; Uchida, T.; Kiefer, B.; Nishiyama, N.; Duffy, T. S., Melting curve of silicon to 15 GPa determined by two-dimensional angle-dispersive diffraction using a Kawai-type apparatus with X-ray transparent sintered diamond anvils. *J. Phys. Chem. Solids* **2008**, *69* (9), 2255-2260.

36. Guignard, J.; Crichton, W. A., The large volume press facility at ID06 beamline of the European synchrotron radiation facility as a High Pressure-High Temperature deformation apparatus. *Rev. Sci. Instrum.* **2015**, *86* (8), 085112.
37. Mayeri, D.; Phillips, B. L.; Augustine, M. P.; Kauzlarich, S. M., NMR Study of the Synthesis of Alkyl-Terminated Silicon Nanoparticles from the Reaction of SiCl<sub>4</sub> with the Zintl Salt, NaSi. *Chemistry of Materials* **2001**, *13* (3), 765-770.
38. Tegze, M.; Hafner, J., Electronic structure of semiconducting alkali-metal silicides and germanides. *Physical Review B* **1989**, *40* (14), 9841-9845.
39. Wang, J.; Sen, S.; Yu, P.; Browning, N. D.; Kauzlarich, S. M., Synthesis and spectroscopic characterization of P-doped Na<sub>4</sub>Si<sub>4</sub>. *Journal of Solid State Chemistry* **2010**, *183* (11), 2522-2527.
40. Mukhanov, V. A.; Solozhenko, V. L., On electrical conductivity of melts of boron and its compounds under pressure. *J. Superhard Mater.* **2015**, *37* (4), 289-291.
41. Dinsdale, A. T., SGTE data for pure elements. *Calphad* **1991**, *15* (4), 317-425.
42. Glazov, V. M.; Shchelikov, O. D., Volume changes during melting and heating of silicon and germanium melts. *High Temperature* **2000**, *38* (3), 405-412.
43. Rhim, W. K.; Chung, S. K.; Rulison, A. J.; Spjut, R. E., Measurements of thermophysical properties of molten silicon by a high-temperature electrostatic levitator. *International Journal of Thermophysics* **1997**, *18* (2), 459-469.
44. Sokolov, P. S.; Mukhanov, V. A.; Chauveau, T.; Solozhenko, V. L., On melting of silicon carbide under pressure. *J. Superhard Mater.* **2012**, *34* (5), 339-341.
45. Hall, H. T., The Melting Point of Germanium as a Function of Pressure to 180,000 Atmospheres. *The Journal of Physical Chemistry* **1955**, *59* (11), 1144-1146.
46. Luedemann, H. D.; Kennedy, G. C., Melting curves of lithium, sodium, potassium, and rubidium to 80 kilobars. *Journal of Geophysical Research* **1968**, *73* (8), 2795-2805.
47. Makarenko, I. N.; Nikolaenko, A. M.; Ivanov, V. A.; Stishov, S. M., Equation of state of alkali metals: Sodium. *JETP* **1975**, *42* (5), 875-879.
48. Wilson, M.; McMillan, P. F., Crystal-Liquid Phase Relations in Silicon at Negative Pressure. *Phys. Rev. Lett.* **2003**, *90* (13), 135703.
49. Daisenberger, D.; McMillan, P. F.; Wilson, M., Crystal-liquid interfaces and phase relations in stable and metastable silicon at positive and negative pressure. *Physical Review B* **2010**, *82* (21), 214101.
50. Christy, A., Isosymmetric structural phase transitions: phenomenology and examples. *Acta Crystallographica Section B* **1995**, *51* (5), 753-757.
51. Solozhenko, V. L.; Kurakevych, O. O., Equilibrium p-T Phase Diagram of Boron: Experimental Study and Thermodynamic Analysis. *Scientific Reports* **2013**, *3*.
52. Yamanaka, S.; Komatsu, M.; Tanaka, M.; Sawa, H.; Inumaru, K., High-Pressure Synthesis and Structural Characterization of the Type II Clathrate Compound Na<sub>30.5</sub>Si<sub>136</sub> Encapsulating Two Sodium Atoms in the Same Silicon Polyhedral Cages. *J. Amer. Chem. Soc.* **2014**, *136* (21), 7717-7725.
53. Clark, S. M.; Zaug, J. M., Compressibility of cubic white, orthorhombic black, rhombohedral black, and simple cubic black phosphorus. *Physical Review B* **2010**, *82* (13), 134111.
54. Bridgman, P. W., TWO NEW MODIFICATIONS OF PHOSPHORUS. *Journal of the American Chemical Society* **1914**, *36* (7), 1344-1363.



## TOC GRAPHICS



The inorganic chemistry of the Na-Si system at high pressure is fascinating, with a large number of interesting compounds accessible in the industrial pressure scale, below 10 GPa. Na<sub>4</sub>Si<sub>4</sub>, a main stable compound in this pressure range and that which is participating in all high-pressure synthetic routes of clathrate silicon frameworks, melts congruently and its melting point increases with pressure with a positive slope.